Mechanical properties of vesicles
II. A model for osmotic swelling and lysis

F. Ross Hallett,* Jackie Marsh,* Bernie G. Nickel,* and Janet M. Wood‡

*Guelph-Waterloo Program for Graduate Work in Physics, ‡Department of Microbiology, University of Guelph, Ontario, Canada, N1G 2W1

ABSTRACT   Vesicle polydispersity and leakage of solutes from the vesicle lumen influence the measurement and analysis of osmotically induced vesicle swelling and lysis, but their effects have not been considered in previous studies of these processes. In this study, a model is developed which expressly includes polydispersity and leakage effects. The companion paper demonstrated the preparation and characterization of large unilamellar lipid vesicles. A dye release technique was employed to indicate the leakage of solutes from the vesicles during osmotic swelling. Changes in vesicle size were monitored by dynamic light scattering (DLS). In explaining the results, the model identifies three stages. The first phase involves differential increases in membrane tension with strain increasing in larger vesicles before smaller ones. In the second phase, the yield point for lysis (leakage) is reached sequentially from large sizes to small sizes. In the final phase, the lumen contents and the external medium partially equilibrate under conditions of constant membrane tension. When fit to the data, the model yields information on polydispersity-corrected values for membrane area compressibility, Young's modulus, and yield point for lysis.

INTRODUCTION

Vesicles are widely used as model systems for the study of both passive and facilitated membrane transport phenomena (Kaback, 1986). In addition, they are becoming widely used for the encapsulation of DNA, drugs, insecticides, herbicides, and food flavorants and colorants (Gregoriadis, 1984). In spite of this widespread interest, and the enhanced ability to control liposome size and composition, technical difficulties related to vesicle polydispersity and permeability have limited the development of quantitative information on these systems. Of specific interest are the mechanical properties that characterize membrane tension and membrane permeability, both of which are influenced by vesicle size. There is a great need for methodologies that support simultaneous (or at least parallel) monitoring of biochemical activities and membrane mechanical properties if we are to test hypotheses linking membrane tension, permeability changes, or channel activities to physiological outcomes. The combined use of dynamic light scattering (DLS) and fluorescence self-quenching spectroscopy, together with the ability to expressly include polydispersity in the analysis of the results, allows this need to be at least partially met.

A variety of techniques have been used in attempts to characterize membrane vesicle elasticity (Rutkowski et al., 1991) and permeability (Ye and Verkman, 1989). Three groups have used dynamic light scattering (DLS) to measure the swelling of vesicles in response to an imposed osmotic pressure gradient (Sun et al., 1986, Hantz et al., 1986, Rutkowski et al., 1991). Their measurements have indicated an increase in radii of no more than 6%, and Young's moduli of 10^7 to $10^8 \, \text{N} \, \text{m}^{-2}$. How-ever, interpretation of light scattering data derived from membrane vesicle samples has been complicated by a number of factors. Theoretical treatments of vesicle osmotic swelling have usually been based on the assumption that vesicle populations have been unilamellar and monodisperse, though such populations are not readily prepared. As well, previous interpretation of vesicle swelling data depends on assumptions regarding the behavior of vesicles that reach (or exceed) their elastic limit, yet parallel measurements of vesicle swelling and lysis have not been reported.

The preceeding article (Ertel et al., 1993) described the preparation of osmolyte-loaded lipid vesicles suitable for swelling and lysis measurements. DLS was used to obtain number distributions of membrane vesicle radii, and nuclear magnetic resonance spectroscopy was used to determine vesicle lamellarity. DLS and fluorescence techniques were then applied in parallel to monitor, respectively, the vesicle swelling and the release of lumenal solutes that accompanied dilution of the vesicles with hypotonic buffer. In this paper those data are shown to be described by a model for membrane stretching and lysis, which encompasses the polydispersity of the sample populations. The model suggests that osmotically induced lysis entails only limited equilibration of vesicle contents with the surrounding medium and a post-lysis vesicle size distribution that is altered by limited vesicle swelling, but not by vesicle fragmentation. Fits of the model to experimental data provide information on the area compressibility, the Youngs's modulus, and the yield points for lysis which are corrected for polydispersity.

THEORETICAL CONSIDERATIONS

We propose a relatively simple model for describing the release of the self-quenching fluorescent dye, 5(6)-car-

Address correspondence to Dr. F. Ross Hallett, Department of Physics, Guelph-Waterloo Program for Graduate Work, University of Guelph, Guelph, Ontario N1G 2W1, Canada.

boxyfluorescein (CF) by vesicles that are subject to hypoosmotic stress. Several alternative models involving complete release through fragmentation, total release through complete equilibration, and partial release through partial equilibration were considered. The only model that was consistent with all the data was the one involving partial release through partial equilibration. This model is based on standard stress/strain expansion of a spherical shell to a yield point at which pore openings allow the dye concentrations of the lumen and the medium to partially equilibrate. Once this occurs, the vesicle is assumed to reseal at a fixed swollen size. These assumptions will be shown to be consistent with both the DLS and the fluorescence results. The vesicle size is shown to be an extremely important parameter for governing the osmotic pressure difference at which lysis occurs. The model is first developed for the monodisperse case. Polydispersity is subsequently included.

If a thin spherical shell such as a vesicle is subject to a net internal excess pressure, the stress on the walls must balance the resultant fluid force. Considering hemispheres,

$$\Delta p \pi r^2 = \sigma 2 \pi r t \qquad (1)$$

$$\sigma = \Delta p \frac{r}{2t} \qquad (2)$$

where σ is the stress, r is the radius of the vesicle, Δp is the pressure difference between the inside and the outside of the vesicles, and t is the wall or membrane thickness. The stress on the membrane wall is resisted by the interactions between the molecules composing it and by the effects of surface tension. The stress is related to the strain (fractional change in surface area A) through the relation,

$$\sigma = k\left(\frac{\Delta A}{A}\right) \qquad (3)$$

in which k is the stretching (Young's) modulus. If $\Delta A / A$ is represented by $((r + \Delta r)^2 - r^2)/r^2$ then for small strain,

$$\sigma = 2k\left(\frac{\Delta r}{r}\right). \qquad (4)$$

The strain increases with the stress until a yield point is reached and leakage begins, possibly through the development of short-lived pores in the membrane. The value of the strain, ϵ^*, at which this happens is represented by

$$\epsilon^* = \left(\frac{\Delta r}{r}\right)^* \qquad (5)$$

The stress, however, was shown in Eq. 2 to be a function of the pressure gradient across the membrane. By equating the right-hand sides of Eqs. 2 and 4,
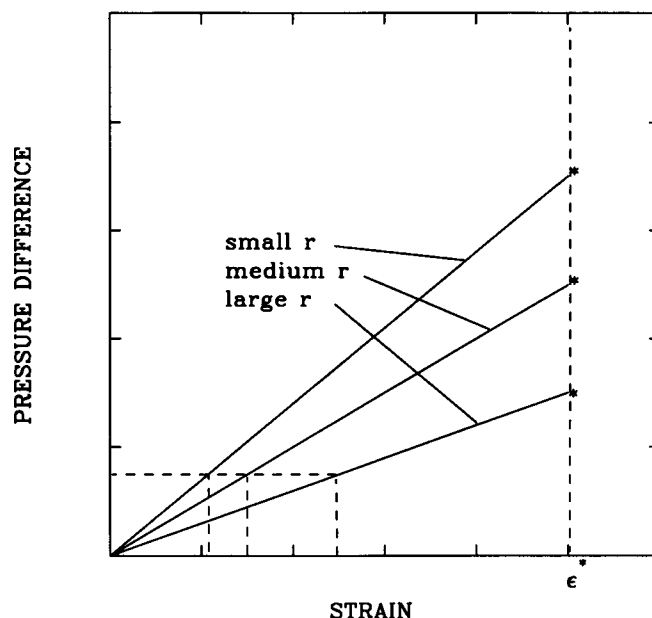

STRAIN

FIGURE 1 The increase in strain with pressure gradient (Eq. 6) depends on vesicle size. The dashed lines at the lower left show that the strain increases with vesicle radius for a fixed pressure gradient. Larger pressure gradients are required to reach the yield point for leakage, ϵ^*, (vertical dashed line on the right) from small vesicles than from large ones.

$$\Delta p = \left(\frac{4kt}{r}\right)\left(\frac{\Delta r}{r}\right). \qquad (6)$$

If the stretching modulus and the membrane thickness are assumed to be constant, then at the yield point

$$\Delta p^* = \left(\frac{4kt}{r^*}\right)\epsilon^* \qquad (7)$$

This result is equivalent to the equilibrium condition first obtained by Katchalsky et al. (1960) for the haemolysing red blood cell. Eqs. 6 and 7 indicate that as the osmotic pressure difference across the vesicle membrane gradually increases, the strain increases linearly to the yield point, but the slope is inversely proportional to the vesicle radius. As the pressure gradient Δp grows (see Fig. 1) larger vesicles reach the yield point ϵ^* before smaller ones. This means that during an experiment in which the osmotic pressure difference across the vesicle wall is gradually increased, a polydisperse population would swell differentially with larger size particles swelling more than smaller ones. Eventual leakage, or lysis of the vesicles, should occur gradually, beginning with the largest and progressing to the smallest sizes in the distribution. This observation is the principle reason that polydispersity must be considered in the interpretation of any measurement involving osmotically induced swelling and leakage of vesicles. These effects of polydisper-
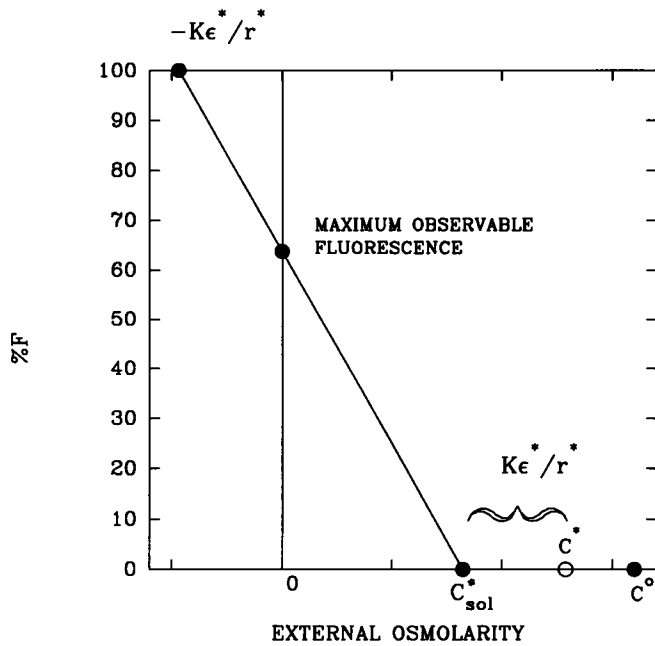
FIGURE 2   The graphical form of Eq. 17 is shown as a function of the external osmolarity C_{sol}. C^0 is the initial osmolarity inside and outside the vesicles. The external osmolarity at which leakage begins and fluorescence begins is C^*_{sol}. The internal osmolarity at the onset of leakage and fluorescence is shown by the hollow circle.

sity will be included at a later stage in the development of the model.

Initially, the vesicle is assumed to have an internal (lumen) solute concentration that is isotonic with the external medium. Thus, the initial internal and external concentrations can both be designated C^0. As the concentration of the external medium, C_{sol}, is gradually diluted from its initial value of C^0, the vesicle radius will increase from its initial value, r, to r^*, at which point leakage or lysis begins. The external concentration at this leakage yield point is C^*_{sol}. While the external concentration falls from C^0 to C^*_{sol}, the internal concentration falls from C^0 to C^*, where,

$$C^* = C^0 \left(\frac{r}{r^*} \right)^3 = \frac{C^0}{(1 + \epsilon^*)^3}. \tag{8}$$

All these concentrations are osmolarities. A fixed fraction, f, of these solutes is the fluorescent dye, which is well above its self-quenching limit at the concentrations,

$$C^0_{dye} = fC^0$$
$$C^*_{dye} = fC^*. \tag{9}$$

The initial dye concentration in the external medium is zero and remains at zero until the external osmolarity reaches the value C^*_{sol} (see Fig. 2.) Below C^*_{sol} vesicles begin to leak their contents. The dye that is released to the medium is not self-quenched, and its concentration

can readily be determined from the intensity of the fluorescent signal. When release begins, the osmotic pressure gradient across the vesicle wall is

$$\Delta p^* = \left(\frac{4kt}{r^*} \right) \epsilon^* = RT(C^* - C^*_{sol}), \tag{10}$$

where R is the gas constant and T is the absolute temperature. Writing

$$K = \frac{4kt}{RT} \tag{11}$$

then,

$$C^* - C^*_{sol} = K \frac{\epsilon^*}{r^*}. \tag{12}$$

The concentration gradient across the membrane remains fixed at this amount as the external concentration is reduced below C^*_{sol}. If C is used to designate the internal concentration in this region, then

$$C - C_{sol} = K \frac{\epsilon^*}{r^*}. \tag{13}$$

The internal concentration, C, continues to drop until C_{sol} reaches zero. Assuming that r^* and f remain constant as C_{sol} falls, the total amount of dye released into the medium is given by

$$Q = \frac{4\pi (r^*)^3}{3} f(C^* - C). \tag{14}$$

Defining the percentage of total dye released, $\%F$, as

$$\%F = 100 \frac{Q}{Q_{max}} \tag{15}$$

where,

$$Q_{max} = \frac{4\pi r^3}{3} fC^0 \tag{16}$$

and combining Eqs. 13, 14, 15, and 16 yields the final expression for percent dye release as a function of external concentration for a monodisperse vesicle system,

$$\%F = 100 \frac{(1 + \epsilon^*)^3}{C^0} \left(C^* - C_{sol} - K \frac{\epsilon^*}{r^*} \right). \tag{17}$$

This is the function graphed in Fig. 2. The intercept at $C_{sol} = 0$ corresponds to the maximum percentage of dye that can be released from a system of intact vesicles by dilution of the external medium. The extrapolated intercept at $C_{sol} = -K\epsilon^*/r^*$ corresponds to the difference between internal and external concentrations at all internal concentrations below C^*.

All liposome preparations are polydisperse and, as mentioned earlier, this polydispersity leads to differen-

tial size changes in response to changing osmotic conditions. Referring to Fig. 1, there are osmotic pressure gradients for which the larger vesicles of a population have reached the yield point and assumed their maximum radius, r^*, whereas vesicles from the small size end of the distribution have just begun to swell. The larger particles are first to lyse as the external concentration is gradually decreased. For a particular value of the external concentration there is a corresponding critical radius for lysis, r^0, where

$$r^0 = \frac{r^*}{(1 + \epsilon^*)} = \frac{K\epsilon^*}{(C^* - C_{sol})(1 + \epsilon^*)} \quad (18)$$

Vesicles smaller than this critical size will not have reached the yield point for lysis. As C_{sol} decreases, the critical radius gradually becomes smaller and smaller until most vesicles in the distribution reach the yield point. To incorporate this polydispersity into the model, it is necessary to average the expression for $\%F$ in Eq. 17 over the radius distribution function $G(r)$. Therefore,

$$\%F = 100(1 + \epsilon^*)^3$$

$$\times \frac{\int_{r^0}^{\infty} r^3 G(r) \left(C^* - C_{sol} - \frac{K\epsilon^*}{(1 + \epsilon^*)r} \right) dr}{C^0 \int_0^{\infty} r^3 G(r) \, dr}. \quad (19)$$

The integral in the denominator corresponds to the total volume of all the vesicles and hence all r, while in the numerator the r are restricted to be greater than the critical radius r^0. Thus,
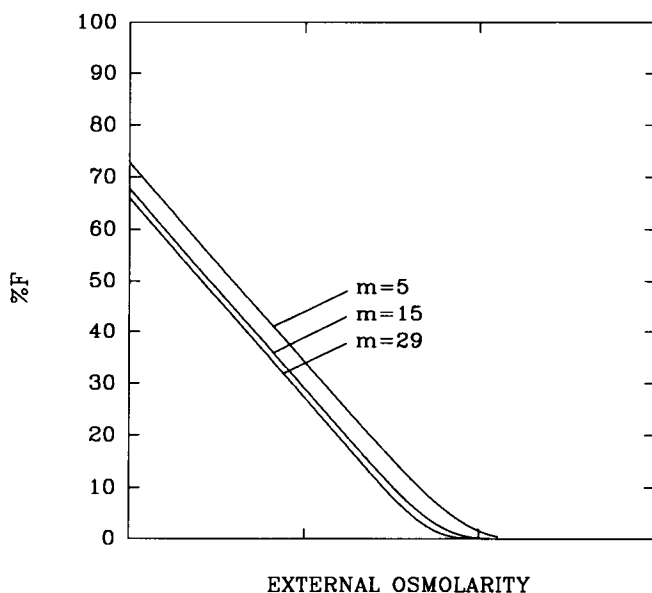

FIGURE 3 The expected dependence of percent fluorescence on external osmolarity, C_{sol}, is shown for three different distributions ($m = 5$, $m = 15$, $m = 29$). The curves were all calculated using Eq. 23, in which only m was varied.

$$\%F = \frac{100}{C^0} (1 + \epsilon^*)^3 (C^* - C_{sol})$$

$$\times \int_{r^0}^{\infty} r^3 G(r) \left(1 - \frac{r^0}{r} \right) dr. \quad (20)$$

In previous studies (Hallett et al., 1991a) we have found that extruded vesicles in the 50- to 100-nm radius range are characterizable by the distribution function (in unnormalized form),

$$G(r) = \frac{r^m}{m!} \exp\left(-r\left(\frac{m + 1}{\bar{r}} \right) \right). \quad (21)$$

The mean of the distribution is determined by $\bar{r}$ and the width by m. Both parameters can be obtained by DLS (Hallett et al., 1991a) or freeze-fracture electron microscopy (Hallett et al., 1991b). Using this expression for $G(r)$ in Eq. 20 yields,

$$\%F = \chi e^{-y} \left(\sum_{i=0}^{m+3} \frac{y^i}{i!} - \frac{r^0}{\bar{r}} \left(\frac{m + 1}{m + 3} \right) \sum_{i=0}^{m+2} \frac{y^i}{i!} \right) \quad (22)$$

or

$$\%F = \chi e^{-y} \sum_{i=0}^{m+2} \left(\frac{m + 3 - i}{m + 3} \right) \frac{y^i}{i!}. \quad (23)$$

This expression can also be written,

$$\%F = \chi \left(1 - \frac{y}{m + 3} \right) - \chi e^{-y} \sum_{i=m+4}^{\infty} \left(\frac{m + 3 - i}{m + 3} \right) \frac{y^i}{i!} \quad (24)$$

where,

$$\chi = \frac{100(1 + \epsilon^*)^3 (C^* - C_{sol})}{C^0} \quad (25)$$

and (see Eq. 18),

$$y = \frac{r^0 (m + 1)}{r} = \frac{K\epsilon^* (m + 1)}{(1 + \epsilon^*)(C^* - C_{sol})\bar{r}}. \quad (26)$$

Fig. 3 shows curves calculated from Eq. 23 for fixed $\bar{r}$ and several values of m. It is clear that polydispersity affects the intercepts and the shape of the curve at high external concentrations. The slopes of the linear regimes are determined only by the value of ϵ^* and are, therefore, the same for all three cases shown. Increasing $\bar{r}$ or decreasing m lead to projected intercepts with the $\%F = 100$ line, which are closer to the origin. Once values of m and $\bar{r}$ are found independently from DLS measurements on the vesicle preparation under isotonic conditions, then the critical radius, r^0 of the radius distribution above which leakage occurs can be obtained from Eq. 26. Eq. 23 can be calculated as a function of C_{sol}. This requires knowledge of K, ϵ^*, and C^*. The value of ϵ^* can be obtained from the slope of the linear region, while the remaining parameters can be obtained from the functional form of the polydispersity corrected intercepts of the straight line segment of Eq. 23. To see this, note that at the small y

limit, which occurs when C_{sol} approaches the asymptotic and artificial limit of $-\infty$, then the second term of Eq. 24 can be dropped and,

$$\% F_{small\, y} = \chi \left(1 - \frac{y}{m + 3} \right) \qquad (27)$$

or

$$\% F_{small\, y} = \frac{100}{C^0} (1 + \epsilon^*)^3$$

$$\times \left(C^* - C_{sol} - \frac{K\epsilon^*(m + 1)}{(1 + \epsilon^*)\bar{r}(m + 3)} \right). \qquad (28)$$

The polydispersity-corrected extrapolated intercept corresponding to $\% F = 100$ occurs when

$$C_{sol} = - \frac{K\epsilon^*(m + 1)}{(1 + \epsilon^*)\bar{r}(m + 3)}, \qquad (29)$$

which corresponds to the monodisperse intercept multiplied by $(m + 1)/(m + 3)$. The $\% F = 0$ intercept of the straight line segment occurs when

$$C_{sol}^* = C^* - \frac{K\epsilon^*(m + 1)}{(1 + \epsilon^*)\bar{r}(m + 3)}. \qquad (30)$$

As a result, K, ϵ^*, and C^* can be obtained by fitting a straight line to the linear section of $\% F$ data measured using the appropriate range of C_{sol}. Since good estimates of t, the membrane thickness, are available from independent x-ray diffraction studies, then the modulus, k, can be determined from K.

The effects of polydispersity can, therefore, be specifically included in the model. It is clear that for very narrow distributions, the equations converge to their monodisperse counterparts. In a later section the model is successfully applied to the swelling and leakage of a fairly narrow distribution of lipid vesicles. It would have been ideal to test the model on broader distributions as well, but it has proven difficult to prepare broader distributions without a significant fraction of the vesicle population being multilamellar. The alternate approach is to extend the model to include multilamellar vesicles. This is presently being attempted.

EXPERIMENTAL METHODS

The preparation of dioleoylphosphatidylglycerol (DOPG) vesicles is described in detail in the companion paper (Ertel et al. 1993). The samples for lysis (50 mg/mL DOPG in 20 mM sodium 3(N-morpholino)propane sulfonic acid (NaMOPS) were extruded through polycarbonate filters of pore radius 50 nm. In addition, 100 mM 5(6)-carboxyfluorescein (CF, the self-quenching fluorescent probe), and 600 mM sodium chloride were added to the medium prior to the freeze/thaw cycles. At this concentration the fluorescence of the dye is almost totally self-quenched. The total osmolarity of the solu-

tion in the vesicle lumen is 1500 mosM plus the additional osmolarity due to the 20 mM NaMOPS. The free probe remaining in the medium was removed from the probe-loaded vesicles by gel filtration chromatography. The chromatographing solution used for this purpose was the isotonic solution containing 750 mM NaCl plus the 20 mM NaMOPS. The lysis experiments were performed by diluting the external medium with a solution containing 20 mM NaMOPS only. The sample was diluted by making step-wise additions of this hypoosmotic buffer and allowing the sample to stir for 5 min at each step before fluorescence readings were taken. Since the 20 mM NaMOPS was always present at the same concentration inside and outside the vesicle, it did not play a role in establishing the osmotic pressure gradient and was not included in the computation of internal and external osmolarities.

The relative loss of ^{31}P signal (RLOS) in the presence of Mn^{2+} (Bergelson and Barsukov, 1977) provides a measure of the average number of lipid bilayers per vesicle. The samples extruded as above and used in this study demonstrated a RLOS of 53.7 ± 2.4%. This is consistent with samples being essentially 100% unilamellar.

The fluorescent probe 5(6)-carboxyfluorescein (CF) was obtained from Sigma Chemical Company (St. Louis, MO) in purified form. This dye is known for its strong self-quenching ability at higher concentrations (Weinstein et al., 1977; Chen and Knutson, 1988). Details on the preparation of this dye and the fluorescence measurements are included in the companion paper (Ertel et al. 1993). Fig. 4 shows the fluorescent intensity of CF at relatively low dye concentrations. Prior to the onset of lysis, the dye concentration in the external medium was essentially zero. As lysis proceeded, dye was released as the solution was diluted. As a consequence, every fluorescence measurement corresponded to a dye concentration of less than 1 μM and was well within the linear region of the fluorescence vs. concentration curve. The fluorescence measurements were performed on a Hitachi F-2000, using an excitation wavelength of 479 nm and an emission wavelength of 520 nm.

The dynamic light scattering experiments used to determine vesicle size distributions have been described in detail earlier (Hallett et al., 1989, 1991a). A model 125A helium-neon laser (Spectra Physics, Mountain View, CA) was focused into a thermally jacketed scattering chamber. The light scattered by the vesicles was detected by an EMI 9863 photomultiplier (EMI Electronics Ltd. Hayes, England) and photon discrimination and counting was performed using a quantum photometer (Model 1140; Princeton Applied Research, Princeton, NJ). The correlator used was a Langley-Ford Model 1096 (Langley-Ford Instruments, Amherst, MA) and the resulting correlation functions were analyzed using Rayleigh–Gans–Debye form factors for hollow spheres in a discrete Laplace inversion routine.
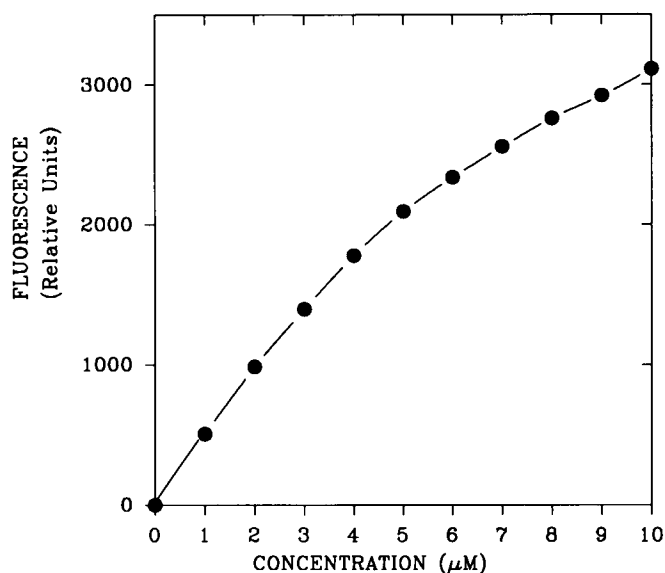
FIGURE 4 The fluorescence of CF as a function of concentration. The solid line is a splines fit to the experimental data points (*solid dots*). Self-quenching is apparent even at dye concentrations as low as 3 μM.
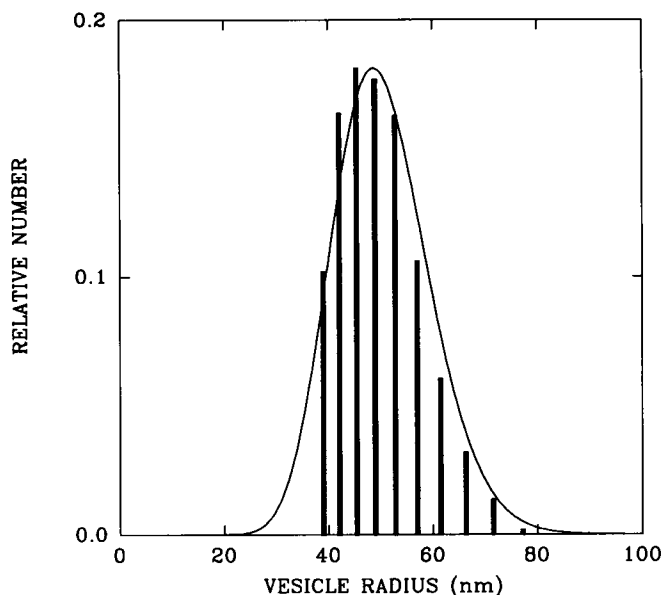

FIGURE 5 The DLS results (*histogram*) obtained from a discrete Laplace inversion of the light-scattering and the best fit distribution (*smooth line*) with the same average radius as the histogram (50.4 nm) and with $m = 29$, calculated using Eq. 21.

RESULTS

The DLS size distribution results from vesicle samples in isotonic medium are shown in histogram form in Fig. 5. Even though it is shown as being discrete, the histogram is completely space filling and represents the smooth number distribution of vesicle radii present in the sample. The average size of the vesicles in this distribution is 50.4 nm. The solid line plotted in Fig. 5 corresponds to the distribution function given by Eq. 11, with $\bar{r}$ set at 50.4 nm and $m = 29$. The value of m was chosen to minimize the least squares differences between the theoretical function and the experimental function from DLS. While the agreement is not perfect, the function represents the experimental results remarkably well.

Fluorescence data from three identical lysis experiments are shown in Fig. 6. The amount of dye released at each dilution is expressed as a percentage (%F) of the maximum releasable dye as obtained by treatment of the maximally diluted sample with Triton X-100. All three data sets demonstrated the overall characteristics predicted by the model described earlier, and approached straight line behavior at lower concentrations of C_{sol} (higher dilutions). A least squares fit of a straight line to this linear section of the data yielded a %F = 0 intercept of 820 ± 40 mosM, a %F = 100 intercept of −470 ± 50 mosM and C_{sol} = 0 intercept of 63.7 ± 1.8%. The internal concentration at which lysis begins C^* is determined (see Fig. 2) to be 820 + 470 = 1290 mosM. This quantity is independent of the vesicle size. That is, lysis begins when the internal concentration reaches this value, regardless of the vesicle size. The slope of the straight line section yields a value for the maximum swelling, ϵ^*, of 0.05 ± .01. This corresponds favorably with the DLS

results taken from equivalent vesicle preparations (see Fig. 7 and Ertel et al., 1993 Table 3). The plateau region correlates with the linear segment of Fig. 6, and provides further corroboration of the model, namely that no further swelling occurs once the yield point for leakage is
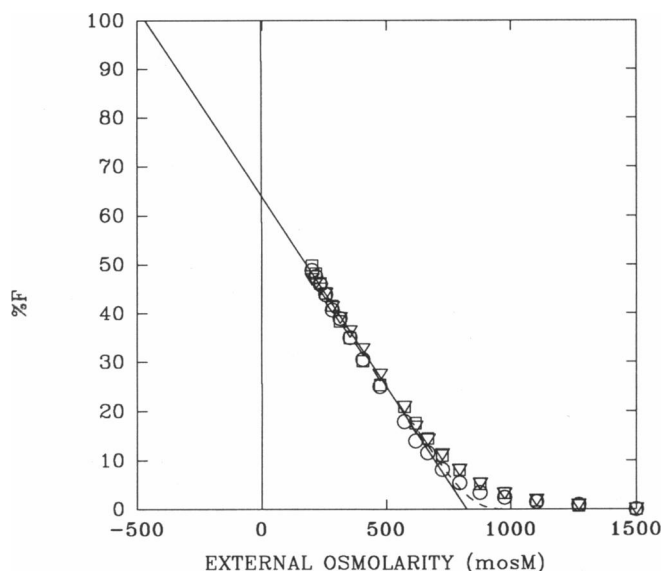

FIGURE 6 The fluorescence data from three identical runs (*circles, triangles, and squares*) per Ertel et al., 1993, Fig. 7, together with the straight line (*solid line*) which best fits the linear segment of the data below 600 mosM. The dashed line is the theoretical function, calculated using Eq. 23 ($m = 29$ and average radius 50.4 nm) which best fits the linear segment of the data.
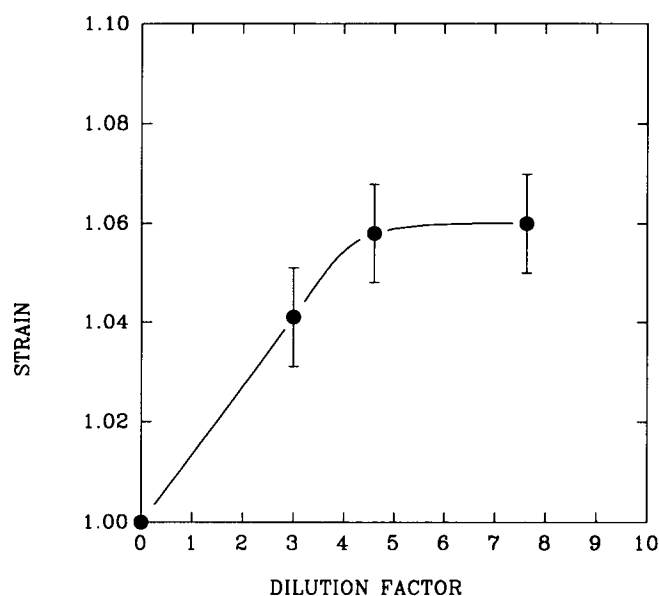
FIGURE 7 The strain, calculated from the DLS data as a function of dilution factor C^0/C_{sol}, per Ertel et al., 1993, Table 3). At greater dilutions the size appears to reach a limiting value. This corresponds approximately to the linear segment of Fig. 6.

reached by all the vesicles in the population. Other groups (Rutkowski et al., 1991) have reported similar amounts of swelling, but did not correlate the swelling with lysis. The curved section of the fluorescence data (Fig. 6) near C^*_{sol} is broader than that expected from the theoretical curve (Fig. 3) for $m = 29$ and $\bar{r} = 50.4$ nm. This may be due to the fact that the yield point is not actually single valued. The reasons for this are not understood but it is possible that the yield point is curvature dependent. Alternatively, fluctuations in the membrane structure might lead to premature changes in membrane permeability and relieve the excess pressure sooner than expected. However, these effects do not affect the determination of the slope of the straight line section and the corresponding intercepts.

Eqs. 11 and 29 allow the calculation of mechanical properties with corrections for polydispersity. Using $\epsilon^* = 0.05$, $\bar{r} = 50.4$ nm, $m = 29$, and the $\%F = 100$ intercept of $C_{sol} = -470$ mosM yields a value for the area compressibility (kt) of 0.34 N m^{-1}. Assuming a membrane thickness (t) of 4.2 nm (Rutkowski et al., 1991) Young's modulus, k, is determined to be 8.2×10^7 N m^{-2}. Table 1 shows this result compared to values from other groups for similar lipid systems. In the case studied here the vesicle distribution is quite narrow and the correction factor for polydispersity $((m + 1)/(m + 3))$ is 0.94. The correction factor could differ significantly from unity for a broader distribution of vesicle sizes.

The analysis indicates that the yield point for lysis in the DOPG vesicles occurs when the strain reaches a value, ϵ^*, of 0.05 or 5%. This is consistent within experimental error to the limiting strain as measured by DLS

(see Fig. 7) of about 6%. While this is a rather small change in radius, the corresponding change in area, $\Delta A / A$, (see Eqs. 3 and 4) is double this or about 10%. An increase in surface area per lipid molecule of 10% could well lead to significant structural perturbations, and pore formation may be one manifestation of these structural changes.

DISCUSSION

A simple model that describes osmotically-induced swelling and lysis has been developed and tested. The approach allows the determination of the mechanical processes and membrane properties associated with the swelling and lysis. Membrane stretching moduli and yield points for lysis can be routinely obtained. Three key regions in the swelling/lysis properties are identified. At external solution concentrations above C^*_{sol} the tension in the membrane is increasing, but no lysis is occurring. At concentrations approaching C^*_{sol} the polydispersity becomes important as vesicles in the size distribution reach the yield point differentially. This is manifested as curvature in the $\%F$ profiles. At concentrations well below C^*_{sol} the $\%F$ curve becomes linear, even in the presence of polydispersity. This is because all vesicles have reached their respective yield points and are leaking their contents. Throughout this linear region the tension in the membrane remains unchanged. Experimenters with interests in following processes that are thought to be sensitive to changes in membrane tension should confine their studies to the region between C^0 and C^*_{sol}. The experimental procedures described in the companion paper and the analytical approach described herein should provide powerful means for selectively determining the mechanical and permeability properties brought about by the insertion of substances into or onto the vesicle membrane. Such substances might include various lipids, including cholesterol, peripheral, or integral membrane proteins that are, or are not, expected to sense or respond to membrane strain, and solvent additives, including membrane stabilizers such as trehalose. These approaches may also permit characterization of the membrane structures through which solutes leak when membranes reach their mechanical yield point.

Our observations (Ertel et al., 1993 and this paper) may have important implications with respect to membrane stabilization in biological systems. In our carefully

TABLE 1 Comparison of mechanical properties of DOPG vesicles

Author	Sample	Area compressibility $(N\,m^{-1})$	Young's modulus $(N\,m^{-2})$
Rutkowski et al., 1991	DOPG (150 mM KCl)	0.220	5.2×10^7
Rutkowski et al., 1991	DOPG (250 mM sucrose)	0.165	3.9×10^7
This work	DOPG	0.34	8.2×10^7

constrained experimental system, large transmembrane osmotic gradients were tolerated as the membranes became strained. The limiting osmotic pressure gradient was then maintained through limited solute leakage without significant perturbation of gross vesicle structure. Other work (for example, that reported in Fig. 4 of Ertel et al., 1993 and summarized by Rutkowski et al., 1991) suggests that larger vesicles and/or vesicles with differing lipid compositions may become much more structurally labile during osmotic swelling. The imposition of membrane strain, like variations in temperature, causes an increase in the surface area per lipid and may potentiate changes in lipid phase behavior that, in turn, destabilize vesicle structure.

Cells and organelles are membrane-bounded structures that are much larger and have much more complex compositions than the extruded DOPG vesicles used in this study. It is generally believed that cell walls serve as scaffolding structures that limit the swelling of cells and organelles, thereby preventing lysis. Cells and organelles may also possess mechanisms, analogous to the solute leakage phenomenon demonstrated here, which limit transmembrane osmotic pressure gradients and thereby stabilize membrane structure. Proteinaceous channels that would respond to membrane strain and open to permit limited solute efflux and thereby maintain transmembrane osmotic pressure gradients below those inducing lipid structural perturbations, could well be used for this purpose. Previously accumulated K^+ ions and betaines are known to be lost rapidly from bacterial, animal, and plant cells as their medium osmolarity is reduced (Booth et al., 1988; Garcia-Perez and Burg, 1991), and mechanosensitive ion channels have been identified in many biological membranes (Morris, 1990). Searches for roles of mechanosensitive ion channels in somoregulation and for mechanosensitive channels that mediate fluxes of non-ionic solutes are suggested by these concepts.

REFERENCES

Bergelson, L. D., and L. I. Barsukov. 1977. Topological asymmetry of phospholipids in membranes. Science (Wash. DC). 197:224–230.

Booth, I. R., J. Cairney, L. Sutherland, and C. F. Higgins. 1988. Enteric bacteria and osmotic stress: an integrated homeostatic system. J. Appl. Bact. Symp. Supp. 35s–49s.

Chen, R. F., and J. R. Knutson. 1988. Mechanism of fluorescence concentration quenching of carboxyfluorescein in liposomes: Energy transfer to nonfluorescent dimers. Anal. Biochem. 72:61–77.

Ertel, A., A. G. Marangoni, J. Marsh, F. R. Hallett, and J. Wood. Mechanical properties of vesicles. I. Coordinated analyses of osmotic swelling and lysis. Biophys. J. 64:000–000.

Garcia-Perez, A., and M. B. Burg. 1991. Role of organic osmolytes in adaptation of renal cells to high osmolarity. J. Membr. Biol. 119:1–13.

Gregoriadis, A., editor. 1984. Vol. 1, Liposome Technology, CRC Press, Boca Raton, FL.

Hallett, F. R., T. Craig, J. Marsh, and B. Nickel. 1989. Particle size analysis: Number distributions by dynamic light scattering. Can. J. Spect. 34:63–70.

Hallett, F. R., J. Watton, and P. Krygsman. 1991a. Vesicle sizing: Number distributions by dynamic light scattering. Biophys. J. 59:357–362.

Hallett, F. R., B. Nickel, C. Samuels, and P. H. Krygsman. 1991b. Determination of vesicle size distributions by freeze-fracture electron microscopy. J. Elect. Mic. Techniques. 17:459–466.

Hantz, E., A. Cao, J. Escaig, and E. Taillandier. 1986. The osmotic response of large unilamellar vesicles studied by quasi-elastic light scattering. Biochim. Biophys. Acta. 862:379–386.

Kaback, H. R. 1986. Active transport in Escherichia coli: passage to permease. Ann. Rev. Biophys. Biophys. Chem. 15:279–319.

Katchalsky, A., O. Kedem, C. Klibansky, and A. de Vries. 1960. Rheological considerations of the haemolysing red blood cell. In Flow Properties of Blood and Other Biological Systems. A. L. Copley and G. Stainsby, editors. Pergamon Press, New York, Oxford, London, Paris. 155–169.

Mayer, L. D., M. J. Hope, and P. R. Cullis. 1986. Vesicles of variable sizes produced by a rapid extrusion procedure. Biochim. Biophys. Acta. 858:161–168.

Morris, C. E. 1990. Mechanosensitive ion channels. J. Membr. Biol. 113:93–107.

Rutkowski, C. A., L. M. Williams, T. H. Haines, and H. Z. Cummins. 1991. The elasticity of synthetic phospholipid vesicles obtained by photon correlation spectroscopy. Biochemistry. 30:5688–5696.

Sun, S.-T., A. Milon, T. Tanaka, G. Ourisson, and Y. Nakatani. 1986. Osmotic swelling of unilamellar vesicles by the stopped-flow light scattering method. Elastic properties of vesicles. Biochim. Biophys. Acta. 860:525–530.

Weinstein, J. N., S. Yoshikami, P. Henkart, R. Blumenthal, and W. A. Hagins. 1977. Liposome-cell interaction. Transfer and intracellular release of a trapped fluorescent marker. Science (Wash. DC). 195:489–491.

Ye, R., and A. S. Verkman. 1989. Simultaneous optical measurement of osmotic and diffusional water permeability in cells and liposomes. Biochemistry. 28:824–829.